

X-ray structure determination

Diffraction data of **1** and **2** were collected at 173(1) K using an Xcalibur diffractometer equipped with MoK α radiation ($\lambda = 0.71073 \text{ \AA}$) and a Sapphire3 detector. Absorption corrections based on the multi-scan method using spherical harmonics, implemented in the SCALE3 ABSPACK scaling algorithm were done with $T_{\min} = 0.536$, $T_{\max} = 1.000$ for **1** and $T_{\min} = 0.9027$, $T_{\max} = 1.0000$ for **2**, respectively. [CrysAlis PRO, Agilent Technologies, Version 1.171.36.28 (release 01-02-2013 CrysAlis171 .NET) (compiled Feb 1 2013,16:14:44) nad].

Data collection: *CrysAlis PRO*, Agilent Technologies, Version 1.171.36.28 (release 01-02-2013 CrysAlis171 .NET) (compiled Feb 1 2013,16:14:44); cell refinement: *CrysAlis PRO*, Agilent Technologies, Version 1.171.36.28 (release 01-02-2013 CrysAlis171 .NET) (compiled Feb 1 2013,16:14:44); data reduction: *CrysAlis PRO*, Agilent Technologies, Version 1.171.36.28 (release 01-02-2013 CrysAlis171 .NET) (compiled Feb 1 2013,16:14:44); program(s) used to solve structure: *SIR* 92; program(s) used to refine structure: *ShelXL* (2016/6). (Sheldrick, 2015); molecular graphics: *DIAMOND* (Brandenburg, 2007); software used to prepare material for publication: *ShelXL* (2016/6). (Sheldrick, 2015).

In both crystal structure refinements the hydrogen atoms from the PDOA ligands were placed at calculated positions and treated using the riding model with U_{iso} tied to 1.2 times U_{eq} of the parent carbon atom. The hydrogen atoms from aqua ligands and water solvate molecules were located in difference maps and their positional parameters were freely refined while their isotropic thermal parameters were constrained to be 1.5 times of the U_{eq} of the parent oxygen atom. The hydrogen atoms from disordered (O15W) and in addition partially occupied (O16W) water solvate molecules were not located.

The bridging PDOA ligand in **2** was found to be disordered over two positions related by a centre of symmetry with equal occupancies for the two positions. In the opposite space with respect to the disordered phenyl ring were located disordered and partially occupied water solvate molecules (see Figure S3). The deposited CIFs include the input instructions and unmerged diffraction data for the final refinements.

Crystallographic data for compounds **1** (CCDC 1523868) and **2** (CCDC 1523869) have been deposited with the Cambridge Crystallographic Data Centre. These can be obtained free of charge from The Cambridge Crystallographic Data Centre via www.ccdc.cam.ac.uk/data_request/cif.

References

- Agilent Technologies (2013). *CrysAlis PRO* Version 1.171.36.28.
A. Altomare, G. Cascarano, C. Giacovazzo, A. Guagliardi, M. C. Burla, G. Polidori and M. Camalli, *J. Appl. Cryst.*, 1994, **27**, 435.
K. Brandenburg, *DIAMOND*. Crystal Impact GbR, Bonn, Germany, 2007.
Sheldrick, G. M. (2015). *Acta Cryst. C71*, 3–8.

Table S1 Possible hydrogen bonds (\AA , $^\circ$) for **1**.

$D-\text{H}\cdots A$	$D-\text{H}$	$\text{H}\cdots A$	$D\cdots A$	$D-\text{H}\cdots A$
O10W—H10C···O6 ^{iv}	0.87(4)	1.95(4)	2.807(3)	168(3)
O10W—H10D···O6 ^v	0.75(4)	1.95(4)	2.691(3)	174(4)
O11W—H11C···O13W	0.84(4)	1.82(4)	2.650(3)	169(3)
O11W—H11D···O1 ⁱ	0.78(4)	1.98(4)	2.719(3)	157(3)
O12W—H12C···O6 ^{vi}	0.76(4)	2.54(4)	3.240(3)	153(3)
O12W—H12D···O5 ^v	0.78(4)	2.11(4)	2.891(3)	173(4)
O13W—H13C···O12W ^{vii}	0.68(4)	2.20(4)	2.872(3)	169(5)
O13W—H13D···O8	0.95(4)	1.74(4)	2.677(3)	173(3)
C2—H2B···O8 ^{iv}	0.99	2.17	3.069(3)	151
C7—H7···O8 ^{vi}	0.95	2.59	3.270(3)	128
C9—H9A···O13W ^{vi}	0.99	2.50	3.449(3)	160

Symmetry codes: (i) x , $1-y$, $z-1/2$; (ii) x , $1-y$, $z+1/2$; (iii) $1-x$, y , $1/2-z$; (iv) $3/2-x$, $y-1/2$, z ; (v) $3/2-x$, $3/2-y$, $z+1/2$; (vi) x , $2-y$, $1/2+z$; (vii) x , y , $z-1$; (viii) $3/2-x$, $3/2-y$, $z-1/2$.

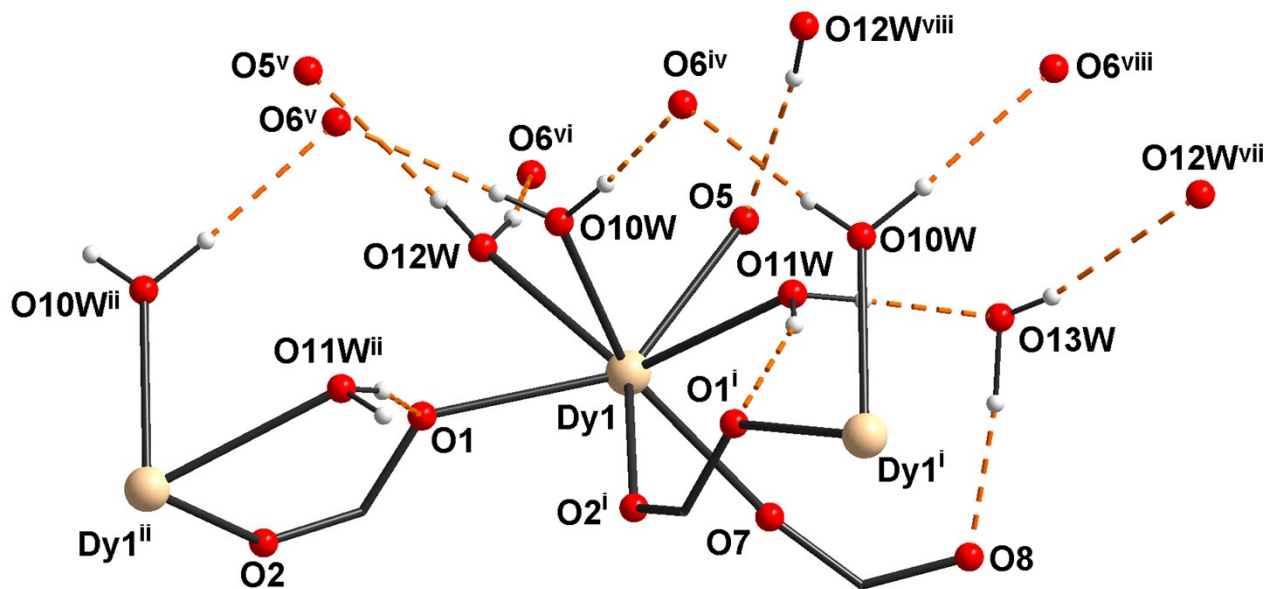


Figure S1 Hydrogen bonding scheme in **1**. Symmetry codes: (i) x , $1-y$, $z-1/2$; (ii) x , $1-y$, $z+1/2$; (iii) $1-x$, y , $1/2-z$; (iv) $3/2-x$, $y-1/2$, z ; (v) $3/2-x$, $3/2-y$, $z+1/2$; (vi) x , $2-y$, $1/2+z$; (vii) x , y , $z-1$; (viii) $3/2-x$, $3/2-y$, $z-1/2$.

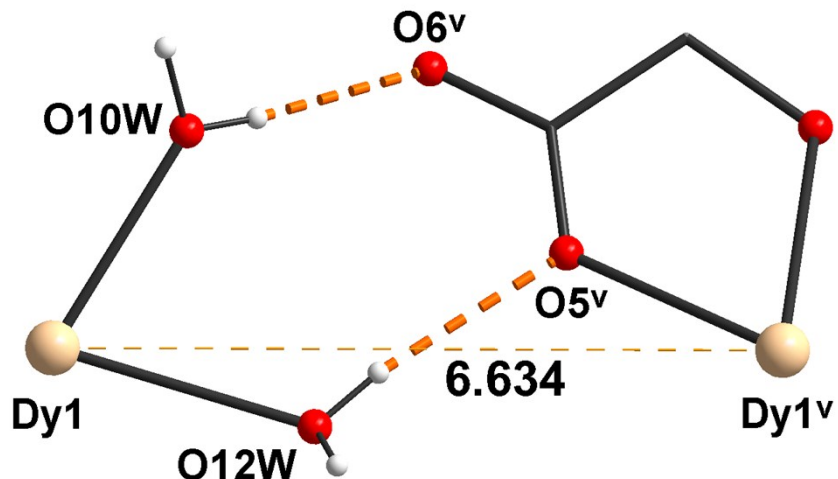


Figure S2 View of shortest interatomic distance of 6.6340(7) Å between Dy(III) atoms linked by hydrogen bonds in **1**. Yellow thick dashed lines represent hydrogen bonds while yellow thin dashed line represents the interatomic distance between the Dy(III) atoms in Å. See also Figures S2 and S3. Symmetry code: (v) 3/2-x, 3/2-y, z+1/2.

Table S2 Possible hydrogen bonds (Å, °) for **2**.

D—H···A	D—H	H···A	D···A	D—H···A
O11W-H11A···O6 ⁱⁱ	0.85(4)	1.96(4)	2.815(5)	173(7)
O11W-H11B···O6 ⁱⁱⁱ	0.86(4)	1.90(5)	2.743(6)	164(6)
O12W-H12C···O1 ^{iv}	0.82(7)	1.91(7)	2.731(5)	174(7)
O12W-H12D···O14W ^{iv}	0.66(7)	2.26(7)	2.911(6)	171(9)
O13W-H13A···O14W	0.72(6)	2.03(6)	2.746(6)	173(8)
O13W-H13B···O2 ^{iv}	0.69(6)	2.03(7)	2.702(5)	165(9)
O14W-H14A···O2 ^v	0.82(8)	1.99(8)	2.814(6)	174(7)
O14W-H14B···O6 ⁱⁱ	0.82(7)	2.10(7)	2.858(6)	152(7)

Symmetry codes: (ii): x, 1+y, z; (iii): 1/2-x, 1/2+y, z; (iv): -x, -1/2+y, 3/2-z; (v): 1/2+x, y, 3/2-z.

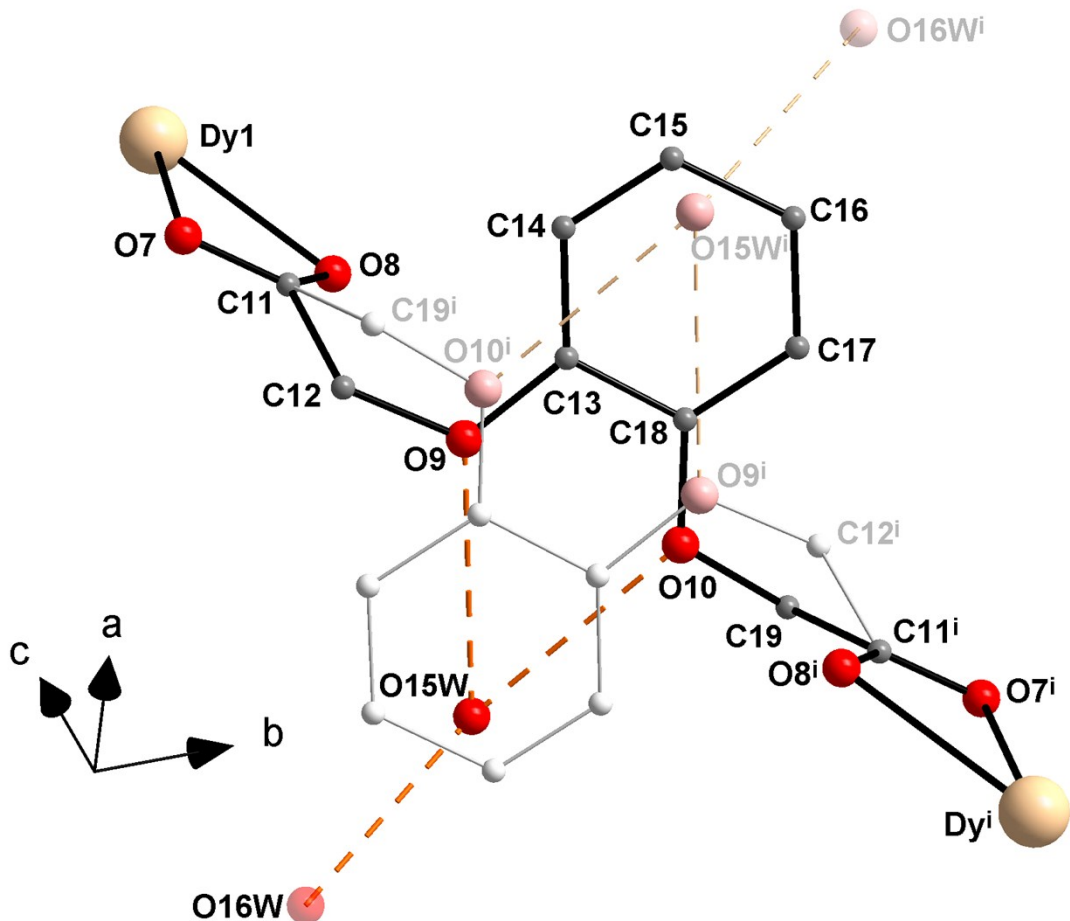


Figure S3 Positional disorder of the bridging PDOA ligand in **2** associated with the disorder of solvate water molecules O15W (s.o.f. = 0.5) and O16W (s.o.f. = 0.25). Dashed lines represent possible hydrogen bonds with distances 3.08(2) Å for O15W...O9, 2.95(3) Å for O15W...O10 and 2.76(3) Å for O16W...O15W. The site occupation factors of the two disordered positions of the PDOA ligand are exactly 0.5 as the two positions are related by a symmetry centre. Symmetry code: (i): -x, 1-y, 1-z.

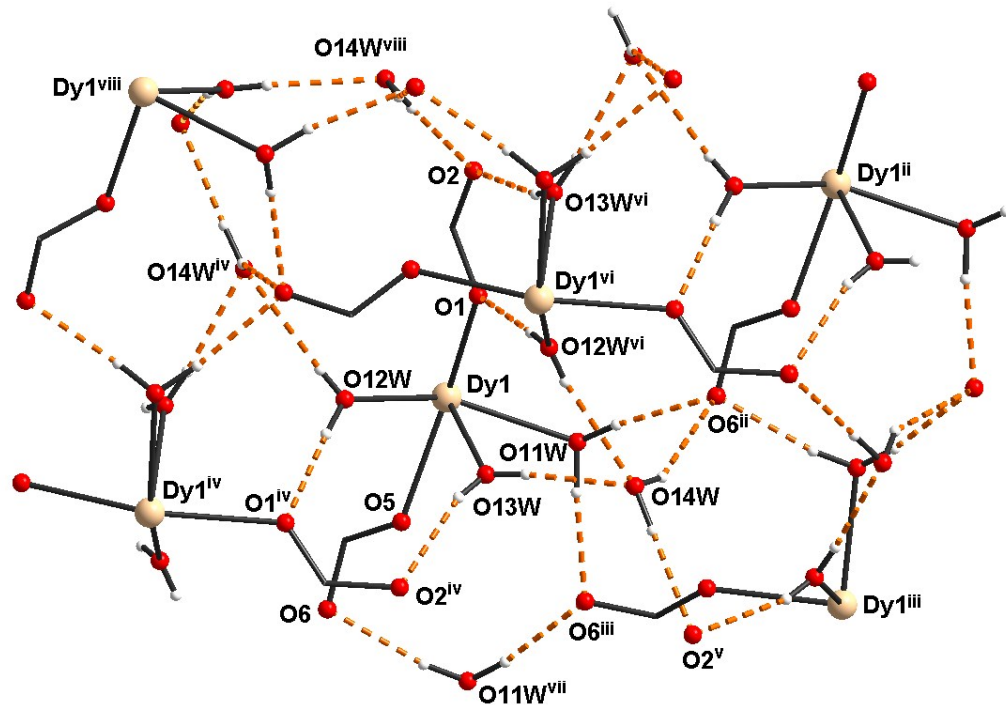


Figure S4 View of the extensive hydrogen bonding scheme in **2**. The disordered water solvate molecules are not shown for clarity. Symmetry codes: (ii): x , $1+y$, z ; (iii): $1/2-x$, $1/2+y$, z ; (iv): $-x$, $y-1/2$, $3/2-z$; (v): $1/2+x$, y , $3/2-z$; (vi): $-x$, $y+1/2$, $3/2-z$; (vii): $1/2-x$, $y-1/2$, z ; (viii): $x-1/2$, y , $3/2-z$.

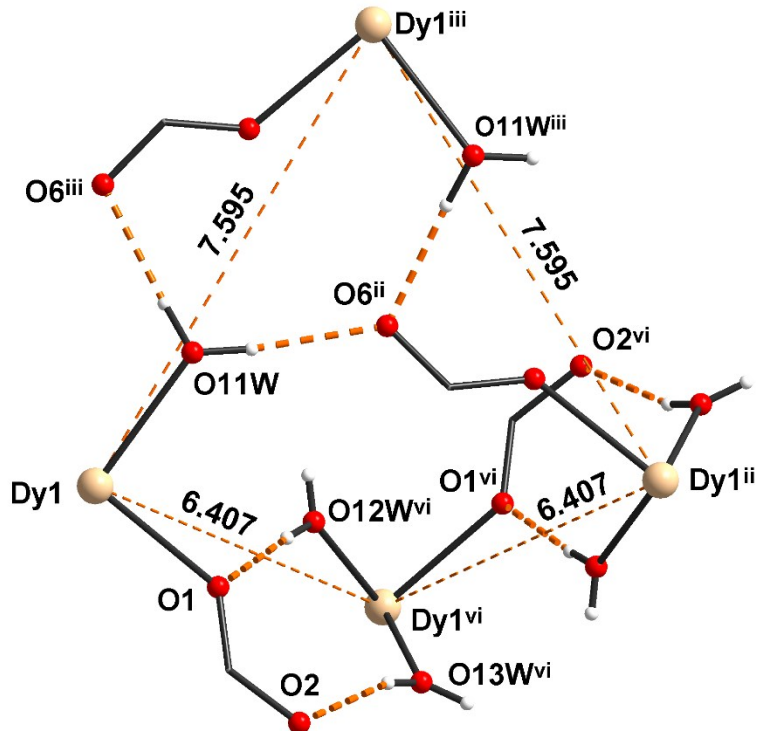


Figure S5 A simplified view of the shortest interatomic distances $6.4074(7)$ and $7.5953(5)$ Å between Dy(III) atoms linked by hydrogen bonds in **2**. Not all hydrogen bonds are shown. Yellow thick dashed

lines represent hydrogen bonds while yellow thin dashed lines represent the interatomic distances between the Dy(III) atoms in Å. Symmetry codes: (ii): x, 1+y, z; (iii): 1/2-x, 1/2+y, z; (vi) -x, y+1/2, 3/2-z.

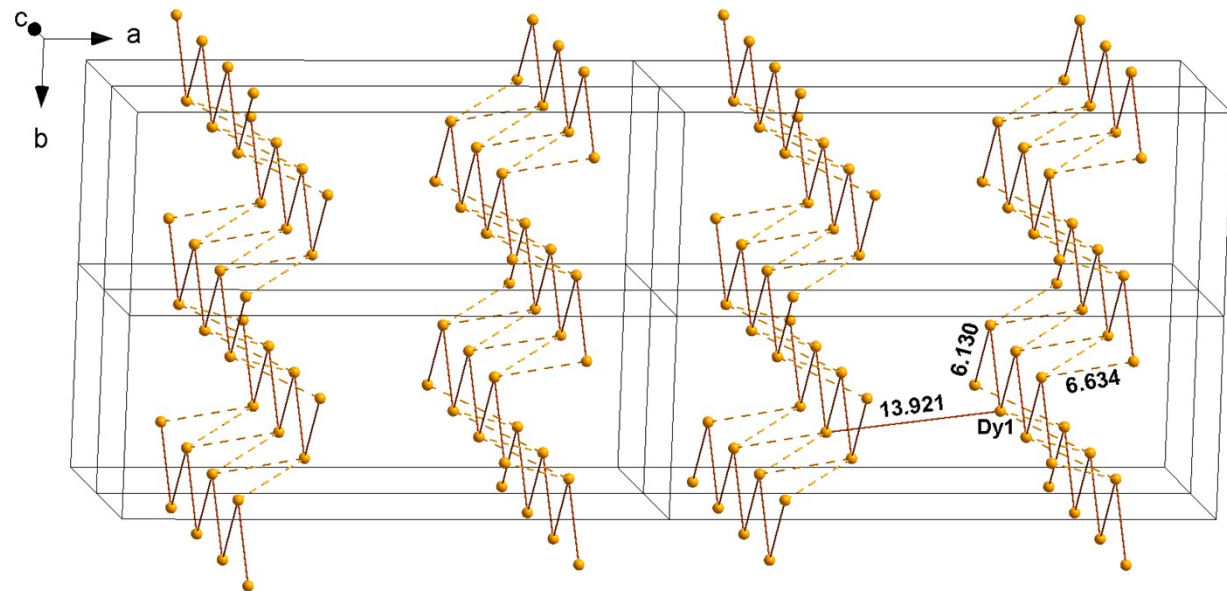


Figure S6 View of the packing of Dy(III) atoms in **1** approximately along *c* axis. The solid brown lines correspond to the short and long bridges based on covalent bonds; only one long bridge (the distance between the Dy(III) atoms is 13.921(9) Å) is displayed for the sake of clarity. The dashed yellow lines correspond to the shortest interatomic distances of 6.1304(9) and 6.6340(7) Å between Dy(III) atoms linked by hydrogen bonding interactions.

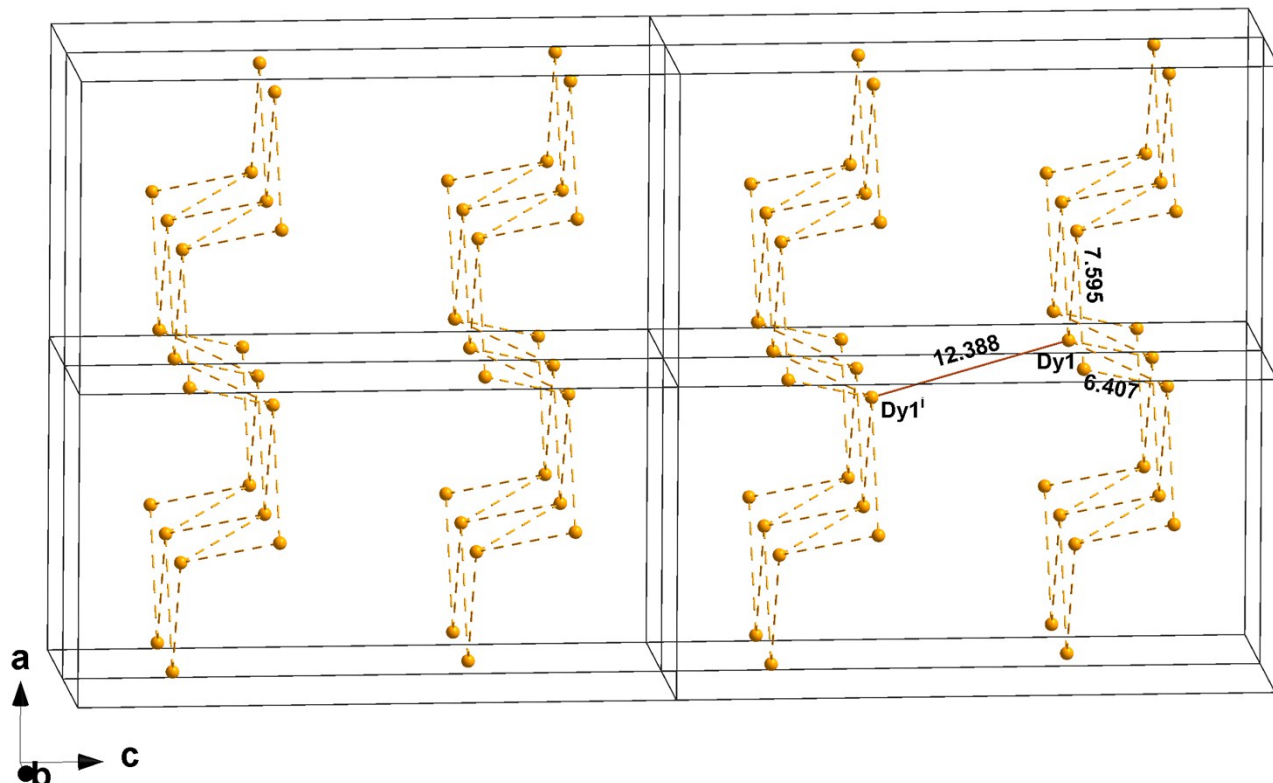


Figure S7 View of the packing of Dy(III) atoms in **2** approximately along the *b* axis. The solid brown line corresponds to the covalently bridged pair of Dy(III) atoms at a distance of 12.3882(9) Å; only one long bridging distance is displayed for the sake of clarity. The dashed yellow lines correspond to the

shortest interatomic distances of 6.4074(7) and 7.5953(5) Å between Dy(III) atoms linked by hydrogen bonding interactions.

DC magnetic data

As suggested elsewhere [K. Zhang, D. Liu, V. Vieru, L. Hou, B. Cui, F.-S. Guo, L. F. Chibotaru, Y.-Y. Wang, Dalton Trans., 2017, 46, 638], the DC susceptibility data for **2** was fitted by using a model of the effective spins $s^* = \frac{1}{2}$ in an exchange interaction

$$\hat{H} = -J(\hat{s}_{1z}^* \cdot \hat{s}_{2z}^*)\hbar^{-2} + \mu_B B g_z (\hat{s}_{1z}^* + \hat{s}_{2z}^*)\hbar^{-1}$$

Though not perfect, this model brings a first insight into the extent of the exchange interaction in the dinuclear complex: $J/hc = -0.5 \text{ cm}^{-1}$, $g_z = 21.9$; some temperature-independent paramagnetism $\chi_{\text{TIP}} \sim 20 \times 10^{-9} \text{ m}^3 \text{ mol}^{-1}$ arises from the presence of low-lying excited states beyond the model. However, the magnetization data cannot be recovered by this set of parameters and they remain heavily underestimated (Figure S8).

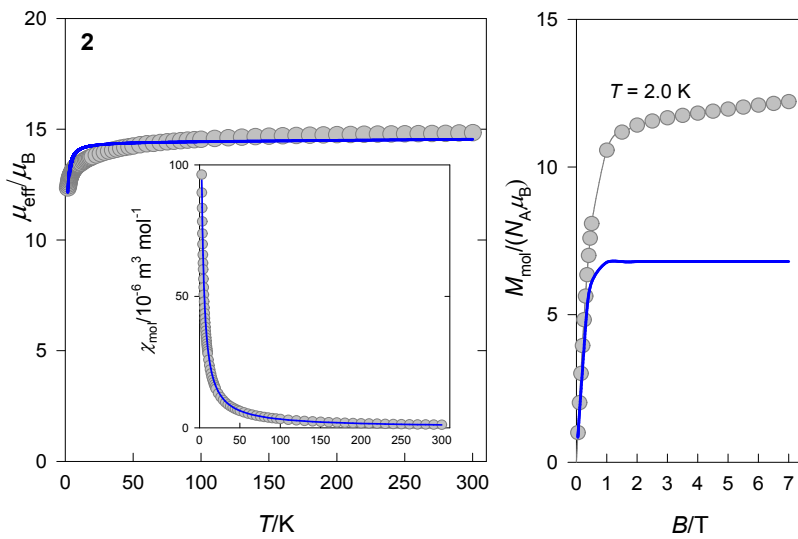


Figure S8 DC data for **2** fitted using the model of the effective spins – see the text above (lines represent the fitted values).

The model has been extended by considering full isotropic exchange interaction and the orientation-dependent Zeeman term (Figure S9)

$$\hat{H}_k = -J(\hat{s}_1^* \cdot \hat{s}_2^*)\hbar^{-2} + \mu_B \hbar^{-1} B [g_z(\hat{s}_{1z}^* + \hat{s}_{2z}^*) \cos \vartheta_k + g_{xy}(\hat{s}_{1x}^* + \hat{s}_{2x}^*) \sin \vartheta_k]$$

yielding $J/hc = -1.25 \text{ cm}^{-1}$, $g_z = 17.1$, $g_{xy} = 8.4$ and $\chi_{\text{TIP}} \sim 50 \times 10^{-9} \text{ m}^3 \text{ mol}^{-1}$

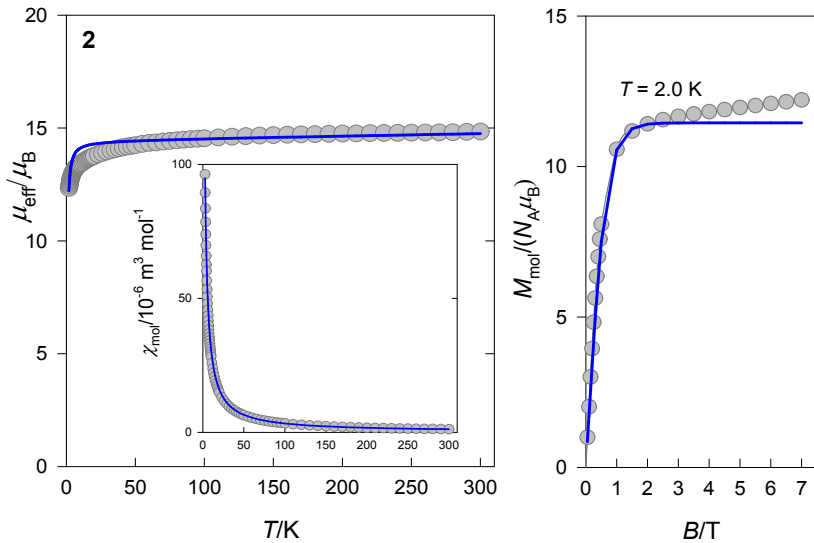


Figure S9 DC data for **2** fitted considering full isotropic exchange interaction and the orientation-dependent Zeeman term (lines represent the fitted values).

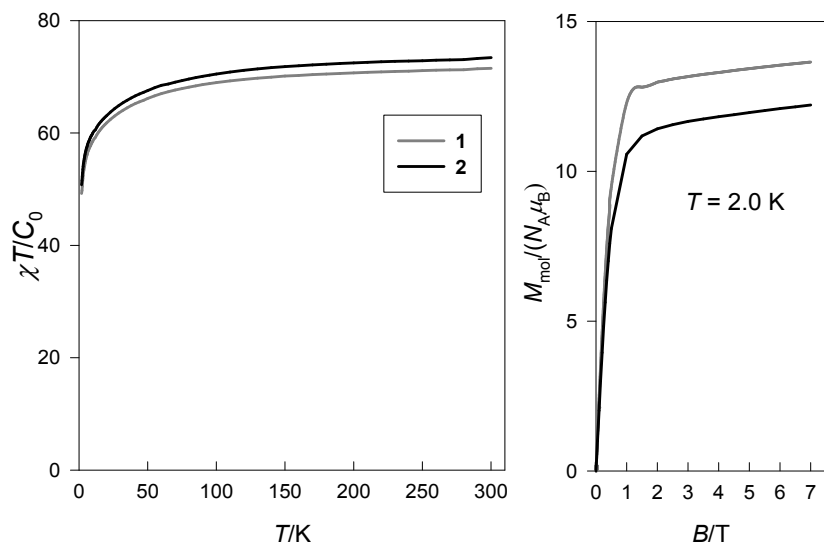


Figure S10 Comparison of DC data for **1** and **2**.

Two components of the AC susceptibility

$$\chi'(\omega) = \chi_s + (\chi_{T1} - \chi_s) \frac{1 + (\omega\tau_1)^{1-\alpha_1} \sin(\pi\alpha_1/2)}{1 + 2(\omega\tau_1)^{1-\alpha_1} \sin(\pi\alpha_1/2) + (\omega\tau_1)^{2-2\alpha_1}} + (\chi_{T2} - \chi_{T1}) \frac{1 + (\omega\tau_2)^{1-\alpha_2} \sin(\pi\alpha_2/2)}{1 + 2(\omega\tau_2)^{1-\alpha_2} \sin(\pi\alpha_2/2) + (\omega\tau_2)^{2-2\alpha_2}}$$

$$\chi''(\omega) = (\chi_{T1} - \chi_s) \frac{(\omega\tau_1)^{1-\alpha_1} \cos(\pi\alpha_1/2)}{1 + 2(\omega\tau_1)^{1-\alpha_1} \sin(\pi\alpha_1/2) + (\omega\tau_1)^{2-2\alpha_1}} + (\chi_{T2} - \chi_{T1}) \frac{(\omega\tau_2)^{1-\alpha_2} \cos(\pi\alpha_2/2)}{1 + 2(\omega\tau_2)^{1-\alpha_2} \sin(\pi\alpha_2/2) + (\omega\tau_2)^{2-2\alpha_2}}$$

Table S3. Parameters of the extended Debye model for **1** using data taken at $B_{DC} = 0.2$ T. ^a

T /K	$R(\chi')$ /%	$R(\chi'')$ /%	χ_s	χ_{T1}	α_1	τ_1 / 10^{-3} s	χ_{T2}	α_2	τ_2 / 10^{-3} s	x_{LF}
a) two-set Debye model										
1.85	0.53	0.56	7.84(28)	89.0(24)	0.19(1)	46.2(10)	114(1)	0.31(2)	1.38(17)	0.76
2.25	1.3	0.64	5.93(72)	78.2(52)	0.22(3)	37.4(23)	107(1)	0.29(5)	0.938(184)	0.72
2.65	1.6	0.53	4.53(106)	62.7(56)	0.20(4)	24.0(20)	96.1(11)	0.28(6)	0.642(112)	0.64
3.95	1.5	0.93	4.17(117)	62.5(75)	0.36(5)	16.2(28)	90.7(16)	0.21(7)	0.368(56)	0.67
3.45	0.45	0.58	2.52(45)	53.1(62)	0.51(4)	15.7(40)	86.6(12)	0.25(3)	0.330(19)	0.60
3.85	0.40	1.4	0.1	37.9(73)	0.60(3)	10.9(72)	79.3(10)	0.30(4)	0.283(12)	0.48
4.25	0.30	0.37	[0]	33.6(16)	0.69(1)	6.3(25)	74.1(9)	0.25(1)	0.229(4)	0.45
4.65	0.61	1.5	[0]	29.7(36)	0.70(4)	1.24(111)	66.8(18)	0.19(4)	0.172(7)	0.44
5.05	0.50	3.3	[0]	20.2(63)	0.70(6)	1.07(216)	61.3(21)	0.18(6)	0.119(1)	0.33
5.45	0.48	4.7	[0]	16.3(91)	0.70(8)	0.57(183)	56.9(21)	0.13(8)	0.084(12)	0.29
b) single-set Debye model										
4.25	3.4	8.1	[0]	-	-	-	61.3(12)	0.36(4)	0.270(43)	
4.65	2.3	5.7	[0]	-	-	-	59.2(7)	0.34(3)	0.178(25)	
5.05	1.9	4.6	[0]	-	-	-	56.2(6)	0.31(3)	0.118(18)	
5.45	1.5	5.1	[0]	-	-	-	52.7(4)	0.26(3)	0.082(15)	
5.85	1.2	4.8	[0]	-	-	-	49.9(3)	0.23(1)	0.0516(14)	
6.25	1.2	7.5	[0]	-	-	-	47.7(3)	0.24(2)	0.0301(15)	
6.65	1.0	7.6	[0]	-	-	-	44.9(2)	0.17(3)	0.0189(13)	
7.05	0.84	8.5	[0]	-	-	-	42.9(2)	0.16(3)	0.0114(11)	

^a SI unit for the molar magnetic susceptibility [10^{-6} m³ mol⁻¹]. [0] – fixed to the zero.

Table S4. Parameters of the extended Debye model for **2** using data taken at $B_{DC} = 0.2$ T. ^a

T /K	$R(\chi')$ /%	$R(\chi'')$ /%	χ_s	χ_{T1}	α_1	τ_1 / 10^{-3} s	χ_{T2}	α_2	τ_2 / 10^{-3} s	x_{LF}
1.9	0.88	3.4	6.5(12)	91.8(41)	0.33(2)	183(8)	131(1)	0.38(4)	1.00(11)	0.69
2.3	0.87	2.6	1.2(16)	61.3(44)	0.28(2)	137(6)	114(1)	0.45(3)	0.765(77)	0.53
2.7	0.67	2.5	0.001	43.9(35)	0.27(2)	102(5)	101(1)	0.45(3)	0.510(33)	0.43
3.1	0.49	1.9	[0]	34.1(80)	0.27(1)	87.6(25)	91.0(3)	0.41(1)	0.227(11)	0.37
3.5	0.46	1.9	[0]	24.1(5)	0.22(1)	91.1(25)	82.0(2)	0.37(1)	0.274(5)	0.29
3.9	0.62	2.5	[0]	16.1(5)	0.19(2)	100(4)	74.8(2)	0.34(1)	0.225(4)	0.22
4.3	0.85	3.9	[0]	11.0(6)	0.19(4)	103(9)	68.7(3)	0.31(1)	0.177(4)	0.16
4.7	0.57	4.6	[0]	7.89(51)	0.20(5)	104(10)	64.3(3)	0.28(1)	0.138(2)	0.12
5.1	0.66	4.9	[0]	6.01(54)	0.25(7)	95.3(144)	59.6(3)	0.24(1)	0.0996(16)	0.10
5.5	0.70	3.9	[0]	4.62(49)	0.29(8)	91.6(174)	56.1(3)	0.21(1)	0.0716(11)	0.08
5.9	0.47	2.3	[0]	3.64(32)	0.34(6)	85.2(145)	52.7(2)	0.18(1)	0.0498(6)	0.07
6.3	0.27	1.7	[0]	2.83(19)	0.38(5)	78.9(103)	49.8(1)	0.15(1)	0.0329(3)	0.06
6.7	0.29	3.5	[0]	2.33(26)	0.44(7)	75.6(175)	47.2(2)	0.13(1)	0.0204(4)	0.05
7.1	0.36	2.0	[0]	1.81(29)	0.47(10)	82.7(280)	44.7(2)	0.14(2)	0.0121(5)	0.04

^a SI unit for the molar magnetic susceptibility [10^{-6} m³ mol⁻¹].

Mole fractions $x_{LF} = (\chi_{T1} - \chi_s)/(\chi_T - \chi_s)$; $x_{HF} = (\chi_{T2} - \chi_{T1})/(\chi_T - \chi_s)$; $\chi_{T2} = \chi_T$ and $x_{HF} = 1 - x_{LF}$.

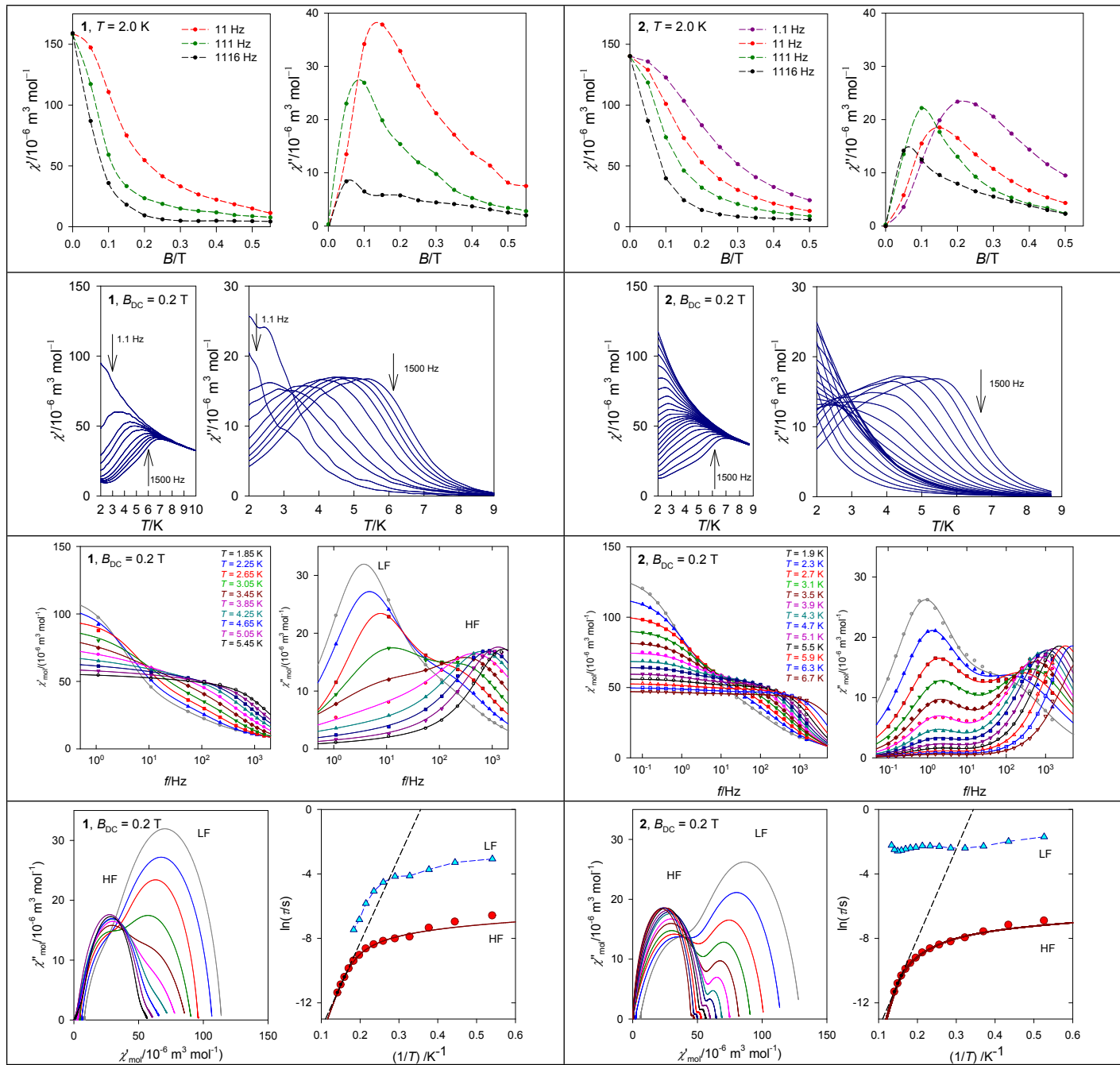


Figure S11 Comparison of AC susceptibility data for **1** and **2**.